# Effective Bifurcation Analysis: A Time-stepper Based Approach

Olof Runborg Constantinos Theodoropoulos
Ioannis G. Kevrekidis

May 16, 2001

## 1 Introduction

In this paper we present a, for the moment heuristic, procedure to perform computer-assisted *effective bifurcation analysis* of dynamics in complex media. Since our terminology is sometimes tentative, we start with a detailed description of what we want to accomplish. *Complex media*, for our purposes, are described by partial differential equations with spatially varying coefficients. Good examples of complex media that exhibit what we term “coarse bifurcations” are (a) two-dimensional composite catalysts surfaces, on which reaction-diffusion processes occur and (b) convection in porous media – what is known as Horton-Rodgers-Lapwood convection or HRLC, [15, 25]. The first example will provide our illustrative case study; the second is chosen to assist our introductory discussion.

Consider a horizontal layer of an isotropic porous medium heated from below. The onset of convection has different descriptions when viewed (a) in experimental detail for a particular realization of a porous medium, [16, 38], and (b) in model equations describing a “homogenized” isotropic porous medium with constant permeability. The first description is truly complicated, very sensitive in its details to the particular realization of the medium and the experimental procedure; the second description is much more simple and elegant: a pitchfork bifurcation for the model PDEs. These model PDEs offer us, then, an “effective” or “coarse” description of the transition; in what follows we will use these two terms interchangeably.

The reason we are able to use dynamical systems language and concepts arising in systems with finite degrees of freedom to describe the transition, is precisely the coarseness of the description – the fact that the behavior has, in some sense, been averaged in space as well as in time. Real experiments in real media can also be modeled in detail. This will give dynamical systems that take into account the actual detailed geometry of the medium, but now the transitions will be immensely more complicated. Actually, the change in dynamic behavior will involve a host of complicated cascades of instabilities in individual pores, and this complexity makes dynamical systems language and bifurcation theory practically useless in capturing and characterizing what "coarsely" happens: the onset of "coarse" convection rolls over an (admittedly narrow) parameter interval that could be thought of as a "coarse bifurcation point".

Clearly, when "system level" information is desired, the complexity of the detailed description is undesirable, and even detrimental. Working with averaged equations gives more insight at what happens "at the system level"; detailed measurements or simulations actually tend to obscure this information. Having the "coarse" equation therefore constitutes a huge boon: not only is it easier to simulate, but it is also easier to understand the results from the simulation in the context of what we practically want to know (say, the critical "coarse" Rayleigh number value). If such equations are available, one should use them in obtaining what we will from now on call "systems level" or "coarse" information about the problem: what the coarse solution looks like (e.g. steady, or periodic) as well as when it has coarse transitions (e.g., onset of convection). It is of course understood that, what is an attracting steady state for the coarse equation may be something much more complex as a dynamical systems object for the detailed problem (*e.g.* a very low amplitude chaotic attractor which in the appropriate averaged variables projects to, essentially, a point, or, for periodic behavior, to a very tight "tube" around a closed curve). It is also understood that what constitutes a sharp bifurcation point for the coarse equations is, really, a very narrow interval in parameter space where, as we discussed above, possibly many detailed transitions occur; these detailed transitions will be different for different realizations of the porous medium. We are, however, not interested in these details. It is the coarse information that we want.

The systems level study of such a complex medium depends crucially on the existence of "coarse" equations. When they are available, we can simulate their behavior: set initial conditions; set parameters, and integrate in time to observe what the long-term dynamics are; change parameters to try and identify transitions, etc. Beyond simulation, we can use the tools of numerical bifurcation theory: Newton-Raphson or other fixed point algorithms to accelerate the location of steady states; eigensolvers to quantify stability; numerical continuation to follow solution branches; algorithms that converge on codimension-one or higher bifurcation points to locate transitions; boundary value solvers to accelerate the location of limit cycles etc.

When effective equations are *not* available, the first path ( detailed direct simulation) is still possible, but, as we argued, not very efficient for obtaining and analyzing "effective", systems level information. Furthermore, when effective equations are not available, the second path (numerical bifurcation calculations) is not viable – we do not have the "coarse right hand sides" (the right-hand-sides of the semi-discretized effective PDEs) or the "coarse Jacobians" (the Jacobians of these semi-discretizations) that we need to perform these tasks.

We propose a computer-assisted procedure which will use short time detailed simulations to perform what amounts to numerical bifurcation analysis of an effective equation *even when this effective equation is not available in closed* *form.* The basic assumption (loosely stated at this point) is that an effective equation *exists* - it is just not available in closed form. For the porous medium problem, for example, our assumption would be that an effective equation in terms of average local fluid momentum, temperature and pressure exist and close (i.e. they constitute a good system level model) – but we do not have these equations (their right hand sides) in any form.

Our procedure is motivated by numerical bifurcation techniques for dissipative PDEs that belong to a family called "time-stepper based methods"; examples of these methods can be found in [44]. In particular, we will build on a technique called the *recursive projection method* (RPM), proposed by Shroff and Keller [39]. These techniques, and RPM in particular, take advantage of the gaps in the spectrum of the linearization of steady states of dissipative PDEs in order to construct contraction mappings based on *time-steppers*: subroutines which, given the state of the system at time $t$, produce a good approximation of the state of the system at time $t+T$. Repeated calls to a time-stepper can be used to adaptively identify a "slow subspace" for the linearization of the system at the steady state. The basic assumption is that this "slow subspace" is low-dimensional: only a few of the eigenvalues of the linearization around the steady state lie close to the imaginary axis, and therefore only a few of the eigenvalues of the linearization of the time-stepper lie in a narrow band around the unit circle in the complex plane. The remaining (many) eigenvalues are far to the left in the left complex plane (the ones of the time-stepper are clustered around zero), with a well-defined gap between these two groups. Then, a Newton-Picard type of iteration, that is, Newton in the low-dimensional slow subspace, and integration (Picard iteration) for the remaining components, is a contraction mapping, [39].

What this practically means, is that the bifurcation analysis of the steady states of a (semi-discretized, dissipative) PDE can be performed using, as the only tool, a time-stepper subroutine for the PDE. The utility of such a technique for better utilization of large legacy codes is obvious, and was, we understand, part of the original motivation for its development.

The crucial (but simple) next step is to realize that the PDE is usually only a simplified model of a certain phenomenon (in the sense that the Navier-Stokes equations constitute a (coarse) model for the evolution of certain moments of the Boltzmann equation, or even of a molecular dynamics simulation of fluid flow). Furthermore, the time-stepper used in the bifurcation calculations can come from the semi-discretized PDE, but it can also come from an alternative computational evolution code, based on alternative (in this case more detailed, microscopic level) models of the same phenomenon.

The "PDE-level time-stepper" takes PDE initial conditions (say, local momenta, temperatures and pressures for the HRLC equations) and returns PDE states (again local momenta, temperatures and pressures) after some time $T$. Alternatively, one can "lift" (embed) a PDE initial condition to an initial condition for an alternative, microscopic description: a molecular initial condition for an MD simulation of a flow field that is *consistent with* the PDE-level initial condition; evolve the microscopic initial condition with microscopic evolution

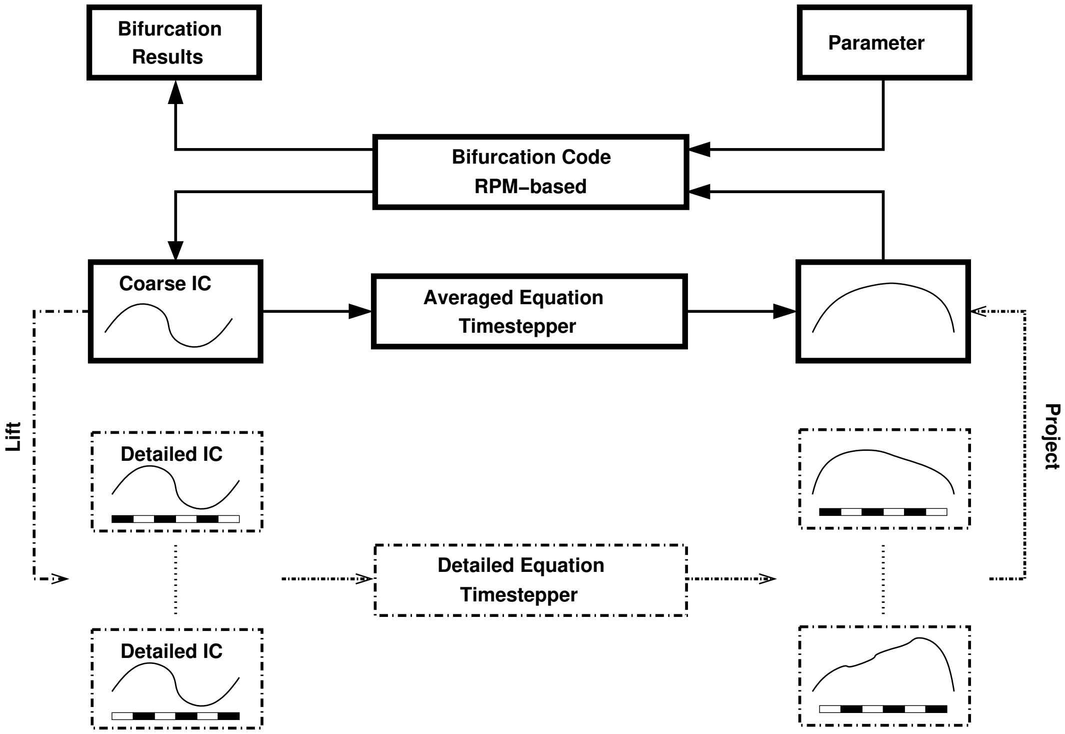


Figure 1: The conceptual process for bifurcation analysis using time-steppers.

rules; and then project the molecular final condition to PDE-level and report it. This idea is described schematically in Figure 1 and has been used in some detail in [42] (a coarse bifurcation analysis of a Lattice-Boltzmann model of the FitzHugh-Nagumo PDE) as well as in [43] (a coarse bifurcation analysis of a Lattice-Boltzmann model of a gas bubble rising in a liquid). Clearly, the process of "lifting" a coarse initial condition to a *consistent* microscopic one is not unique; and, as discussed in these papers, often ensembles of consistent microscopic initial conditions should be evolved, and the average result reported as the output of this "microscopically implemented" coarse time-stepper.

The final step in our train of thought may now be obvious to the reader: suppose that we have one or more realizations of "the same" (in terms of HRLC level modeling) porous medium; that we believe that the HRLC equations exist, close, are dissipative, and constitute a good effective model.

If we have the HRLC equations for our medium, we can perform their bifurcation analysis using the time-stepper approach (e.g. RPM). If we do not have them (but believe they exist) we can very well approximate what their time-stepper would have been by lifting an HRLC-level initial condition to an ensemble of consistent detailed porous medium initial conditions, run the Navier-Stokes in the detailed porous medium for the same amount of time, average the results and project to HRLC-level final conditions. If we use a large enough ensemble of such consistent initial conditions, and if the reporting horizon of the time-stepper, $T$, is chosen within reasonable limits (long enough for errors in "lifting" to relax, and short enough for coarse instabilities not to "explode") we expect the RPM procedure to actually converge. What it converges to should correspond to the fixed point of an (existing but unavailable in closed form) effective equation. We could describe this procedure as an "unavailable model motivated post-processing" of short-term microscopic (in this case, detailed porous medium) simulations.

We will reserve further discussion of the procedure until the end of the paper, after some results have been presented. Our presentation is organized as follows. In Section 2 we will describe the way we coarsen the detailed solution (and, in particular, the "coarse time-stepper"). The flow-chart of the RPM based numerical method is reiterated in Section 3 and our illustrative example and its phenomenology is described in Section 4. Section 5 contains the bulk of our computations, and is followed by a discussion.

## 2 The Coarse Time-stepper

The computational procedure we propose hinges upon a view of the dynamics provided by an important object: the "coarse time stepper". We describe, in reasonably general terms, how to construct this object and the "coarse dynamics" associated with it, as they arise from a detailed equation and its detailed dynamics. Consider a general evolution equation for $u(t, x)$,

$$u_t = F(x, D^\alpha u), \tag{1}$$

where $F$ depends on $x$ in a complicated way (for example, this would reflect the complicated geometry of a composite material) and $D^\alpha u$ represents all spatial derivatives of $u$ up to some order. We introduce $\bar{u}^T(x)$, the *coarse solution* of (1) at $T$. $T$ is a free parameter; our procedure will make sense over a range of $T$ values determined by the different time scales in the detailed problem. For a given initial data $u_0(x)$, we define $\bar{u}^T(x)$ as follows. The initial data $u_0(x)$ is first "lifted" to an ensemble by shifting it evenly over the whole real axis: $u(0, x, s) = u_0(x - s), s \in \mathbb{R}$ . This ensemble of initial data is evolved till time $T$ according to the PDE (1) and it generates thus an ensemble of solutions $u(T, x, s)$ at time $T$. Those solutions are then realigned, i.e. backshifted by the exact same amount $s$ as the corresponding initial data. Finally the solutions are "projected" by averaging over the ensemble (over s). More precisely, we let

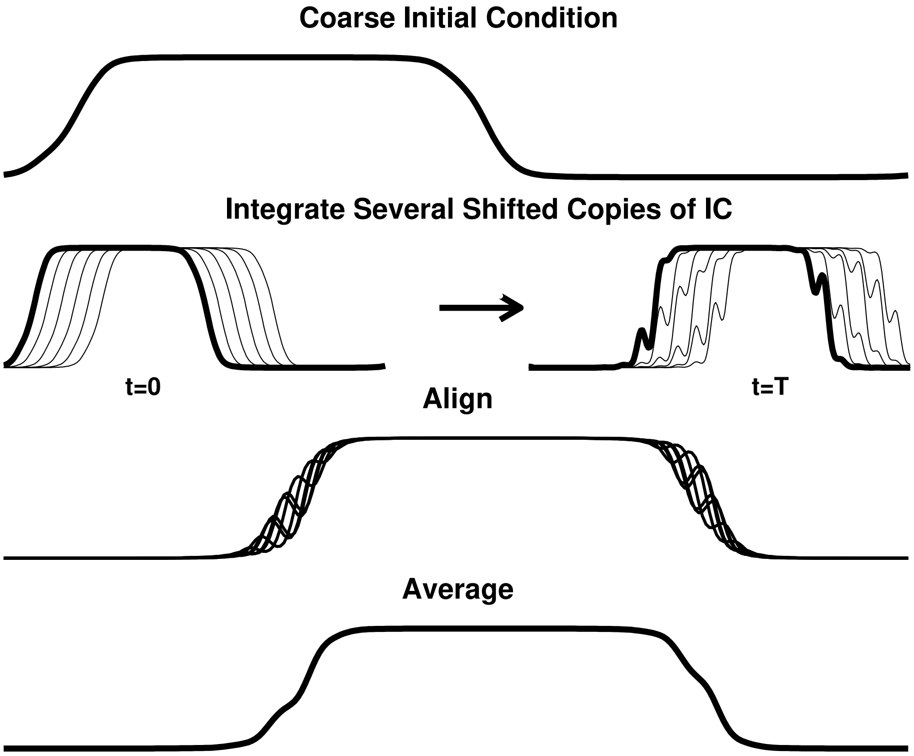


Figure 2: The steps in the averaging procedure.

$\bar{u}^T(x)$ be given by

$$\begin{aligned} \bar{u}^T(x) &\equiv \lim_{R\to\infty} \frac{1}{2R}\int_{-R}^{R} u(T, x+s, s)ds, \\ u_t(t,x,s) &= F(x, D^\alpha u(t,x,s)), \qquad 0 < t < T, \\ u(0,x,s) &= u_0(x-s), \end{aligned} \tag{2}$$

for some initial data $u_0$. See Figure 2 for a schematic description of the procedure. Instead of considering shifts of the initial data, one can formulate the construction of the ensemble through shifting "the underlying material", i.e. move the $s$-shift from the initial data to the function $F$. This amounts to renaming $u(t,x,s) \mapsto u(t,x+s,s)$, leading to

$$\begin{aligned} \bar{u}^T(x) &\equiv \lim_{R\to\infty} \frac{1}{2R}\int_{-R}^{R} u(T, x, s)ds, \\ u_t(t,x,s) &= F(x+s, D^\alpha u(t,x,s)), \qquad 0 < t < T, \\ u(0,x,s) &= u_0(x). \end{aligned} \tag{3}$$

This lends itself to a new interpretation. If we think of $s$ as a stochastic variable uniformly distributed in $\mathbb{R}$, then $\bar{u}^T$ is the expected value of $u$ at time $T$ with respect to $s$ conditioned upon the initial data. Equivalently, $\bar{u}^T$ has the *expected shape* of the solution at time $T$ conditioned upon initial shape $u_0(x)$ randomly positioned on the $x$-axis ($u_0(x+s)$, $s \in \mathbb{R}$). For $n > 0$ we define $\bar{u}^{nT}(x)$ recursively by applying the same construction, but replacing $u_0$ by $\bar{u}^{(n-1)T}$. Hence,

$$
\begin{aligned}
\bar{u}^{nT}(x) &\equiv \lim_{R\to\infty} \frac{1}{2R}\int_{-R}^{R} u(T, x+s, s)ds, \\
u_t(t,x,s) &= F(x, D^{\alpha}u(t,x,s)), \qquad 0 < t < T, \\
u(0,x,s) &= \begin{cases} \bar{u}^{(n-1)T}(x-s), & n > 0, \\ u_0(x-s), & n = 0. \end{cases}
\end{aligned}
\tag{4}
$$

The hope is that the coarse solutions $\bar{u}^{nT}$ at these discrete points in time "come from" a semigroup: that a closed evolution equation –a right hand side– exists, in terms of $\bar{u}(t,x)$ for all $t$; and that $\bar{u}(nT,x) = \bar{u}^{nT}(x)$. This procedure is a natural one, and easy to realize numerically, with concomitant obvious advantages in terms of massive parallelism (each shift is run independently on a different processor). Such a procedure has been employed for the construction of averaged equations from coarse-graining the master equation (e.g. [33, 1]), and, similarly, for the derivation of hydrodynamic descriptions of interacting particle systems (e.g. [28, 27]). It is not clear to us, at this point, that the mathematical derivation for the case of coarse-graining master equations in chemical kinetics, can be extended to the derivation of averaged equations for heterogeneous problems. The purpose of this paper is to provide illustrations and computational collateral for this idea, suggesting a program for the proof of existence of a semigroup for such a procedure. Clearly the hope is that, under appropriate assumptions, the evolution constructed this way, and its long-term dynamics, will be approximated by the evolution of the various levels of homogenized equations and their long-term attractors. Note that, by construction, our dynamics for $\bar{u}^{nT}$ is translationally invariant, as one might also expect from homogenized equations.

The most important point, in terms of added value, in our work comes from the way that we will use this "coarse time-stepper". We will not use it to prove the existence of a semigroup; nor will we use it repeatedly ("bootstrapping" the procedure into the future) to simulate the coarse evolution $\bar{u}^T(x), \ldots, \bar{u}^{nT}(x)$. We will make use of the coarse time-stepper in an alternative context, that will enable us to perform stability and bifurcation analysis of the (unavailable) coarse evolution equation. The method of choice in this paper for such an "intelligent" use of the time-stepper is the RPM method.

# 3 Method

We propose a numerical method for "coarse" bifurcation analysis for steady states of PDEs (whose detailed solutions exhibit multiple scale behavior). The method is described here for evolution equations like (1) where $F$ also depends on a parameter $\lambda$,

$$u_t(t, x; \lambda) = F(x, D^\alpha u; \lambda). \tag{5}$$

The coarse part of $u$ will be denoted $\bar{u}(t, x; \lambda)$ and – based on the above discussion – at time $t = nT$ it is defined to be $u^T(x; \lambda)$. What we are interested in is, hence, bifurcation analysis of attractors of $\bar{u}$ with respect to $\lambda$.

The procedure is based on two observations. The first observation is a fact from numerical analysis: given only a numerical time-stepper code for a dissipative PDE with a steady state, it is possible (under some reasonable conditions) to perform bifurcation analysis for this steady state solution using RPM. The second observation is that, even though we may not be able to write down the explicit equation for $\bar{u}$, our definition of $\bar{u}$ allows us to realize its time-stepper numerically in a straightforward fashion. In effect we construct (appropriately computing the $u$ dynamics) the time-stepper code for $\bar{u}$ that RPM needs to perform the $\bar{u}$ bifurcation analysis.

## 3.1 Bifurcation Analysis with RPM

RPM is an iterative procedure for solving non-linear systems of equations (in particular, discretized PDEs) with some attractive properties. As a tool, RPM has nothing to do with complex medium problems; it is just an acceleration technique for the solution of nonlinear equations (and to stabilize unstable numerical procedures, as it was first presented). The information in this section is therefore just a prerequisite for the later extension to effective bifurcation calculations.

Consider the fixed point problem

$$G(u; \lambda) = u, \tag{6}$$

and let $J$ be the jacobian of $G$.

- Like the Newton method, RPM converges rapidly to the fixed point solution $u_s$ provided the initial guess is good enough; the convergence occurs even if $J(u_s)$ has a few eigenvalues slightly larger than one. The computational cost and convergence rate depends on the eigenvalues of $J$. Optimally there should be a clear gap in the spectrum between small and large (near the unit circle) eigenvalues and a limited number of large (in norm) eigenvalues for RPM to perform well.

- $J$ never needs to be evaluated directly, only $G$. We can therefore apply RPM to any "black box" code that defines a function $G$.

- As a by-product, RPM also computes *approximations of* the largest eigenvalues of $J$. This gives stability information about the fixed point.

When RPM is used for bifurcation analysis of steady states of (usually dissipative evolution) PDEs, the function $G$ represents a *time-stepper*: a subroutine that takes initial data and reports the solution of the PDE after some fixed time (the reporting horizon $T$). A steady state then satisfies (6). The conventional way of finding the steady state using a time-stepper would be to call it many times in succession – in effect, to integrate the PDE for a long time, corresponding to solving (6) by simple fixed point (Picard) iterations.

RPM improves this approach in two important respects. First, the convergence can be significantly accelerated. The nature of the transport PDEs we usually encounter (the action of viscosity, heat conduction, diffusion, and the resulting spectra) ensures that there exists a separation of time-scales, which translates into an eigenvalue gap in the spectrum of $J$ at the steady state. Second, RPM converges even if the steady state is slightly unstable, i.e. when $J$ has a few eigenvalues outside (but still not too far from) the unit circle. It is hence possible to compute unsteady branches of the bifurcation diagram using forward integration (but in a nonconventional way, dictated by the RPM protocol).

RPM still retains the simplicity of the fixed point iteration, in the sense that no more information is needed than just the time-integrator code. This code, which may be a legacy code, and can incorporate the best physics and modeling available for the process, is used by RPM as a black box.

RPM can be seen as a modified version of fixed point iteration. It adaptively identifies the subspace corresponding to large (in norm) eigenvalues of $J$, hence the directions of slow or unstable time-evolution in phase space. In these directions the fixed-point iteration is replaced by Newton iteration. More precisely, suppose $G : \mathbb{R}^N \times \mathbb{R} \mapsto \mathbb{R}^N$ in (6). Let $\mathbb{P}$ be the maximal invariant subspace of $J$ corresponding to the $m$ largest eigenvalues and let $\mathbb{Q}$ be its orthogonal complement in $\mathbb{R}^N$. The solution $u$ is decomposed as $u = p + q = Pu + Qu$, where $P$ and $Q$, are the projection operators in $\mathbb{R}^N$ on $\mathbb{P}$ and $\mathbb{Q}$. Furthermore, define

$$f(p, q; \lambda) \equiv PG(p + q; \lambda), \qquad g(p, q; \lambda) \equiv QG(p + q; \lambda),$$

and

$$j(p, q; \lambda) \equiv PJ(p + q; \lambda)P.$$

Then, the RPM iteration is

$$\begin{aligned} p^{n+1} &= p^n - \Big(j(p^n, q^n; \lambda) - I\Big)^{-1} \Big(f(p^n, q^n; \lambda) - p^n\Big), \\ q^{n+1} &= g(p^n, q^n; \lambda), \end{aligned}$$

and $u_n \equiv p^n + q^n$ converges to the solution of (6) under the right assumptions. If the number of large eigenvalues, $m$, is limited, the dimension of $\mathbb{P}$ and the subspace Jacobian in the Newton iteration, $j - I$, remains small. Only this small Jacobian needs to be approximated and inverted. For a more complete description of RPM we refer to [39].

Going beyond finding steady states as fixed points of the time-stepper, RPM can be modified [39] to work with the augmented systems of algebraic equations involved in (pseudo-arclength) continuation. It can also be used in phase$\times$parameter space fixed point algorithms for the location of codimension-1 and even higher codimension bifurcation points (see [7, 8, 24, 13] for a review of current practice in such calculations). In this context, RPM can be (and has been) used to perform the time-stepper based bifurcation analysis of a number of dissipative PDEs including the Navier-Stokes equations [39, 42, 30, 31, 19].

### 3.2 Extension to Effective Bifurcation Analysis

Conceptually, the RPM-based bifurcation analysis can be described by Figure 1. In the usual setting we have a time-stepper code for some PDE, and this furnishes us with the $G$ in (6). To perform "effective" or "coarse" bifurcation analysis, we therefore need a time-stepper code for the *effective* equation corresponding to (5). Since we typically do not have this equation in an explicit form, we simply propose to replace the time-stepping code by something more complicated, but straightforwardly realizable, namely the coarse time-stepper described in Section 2.

It is important to note here that, for the procedure to be computationally efficient, the (unavailable) effective equation linearized around the PDE steady state(s) of interest, should have a few eigenvalues in a band around the imaginary axis, and the remaining ones should be far to the left of this band. This implies that the effective PDE should be, among other things, dissipative.

## 4 Test Problem

Since we are interested in long-term dynamics (attractors and bifurcations) we choose as an example to study pattern formation in nonuniform reactive media. Since the discovery of the Belousov-Zhabotinskii reaction, reaction-diffusion problems have provided a testbed for the experimental and computational study of pattern formation, [6]. In particular, the study of $CO$ oxidation over single metal crystal catalyst surfaces has provided some of the most spectacular experimental observations of spiral waves, target patterns, traveling waves and fronts, as well as "chemical turbulence" [9, 14, 26, 32, 35]. Over the last several years we have studied the spatiotemporal dynamics of this catalytic reaction on *microsctructured composite catalysts*: catalytic surfaces consisting of, say, alternating stripes of two different catalysts, like Platinum, $Pt$, and Palladium, $Pd$, or Platinum and Rhodium, $Rh$ [14, 3, 41, 10, 37]. The idea is to combine the catalytic activities of the different metals, which are coupled through surface diffusion, to produce a catalyst with improved average reactivity or selectivity. For the purposes of this paper, $CO$ oxidation over such a composite medium is qualitatively described through a system of two coupled partial differential equations,

$$\begin{aligned} u_t &= u_{xx} + \frac{1}{\varepsilon} u(1-u)\left(u - \frac{w+b(x)}{a(x)}\right), \\ w_t &= g(u) - w, \end{aligned} \tag{7}$$

with

$$g(u) = \begin{cases} 0, & u < 1/3, \\ 1 - 6.75\, u(u-1)^2, & 1/3 \le u < 1, \\ 1, & u \ge 1. \end{cases} \tag{8}$$

Here $u$ corresponds to the surface concentration of $CO$, $w$ is a so-called surface reconstruction variable, and $g(u)$ is an experimentally fitted sigmoidal function. Details of the mechanistic modeling as well as the procedure for obtaining this rather successful qualitative caricature model can be found in [17, 2].

In this model $a$, $b$, and the time-scales ratio parameter $\varepsilon$ are physical parameters that incorporate the experimental conditions: partial pressures of $O_2$ and $CO$ in the gas phase, temperature, as well as kinetic constants for the surface. When $a$ and $b$ are spatially uniform (a single uniform catalyst) it is well-known that (7) can fall in the so-called "excitable regime" and support stable traveling pulses. In our case we will study a box of length $L$ with a *periodically varying* medium: a striped surface that can be thought of as consisting of equal amounts of $Pt$ and $Rh$, with stripe width $\lambda/2$ (wavelength $\lambda$). The medium is thus defined by

$$a(x) = \text{const} = 0.84, \qquad b(x) = -0.025 + 0.725 \sin\left(\frac{2\pi x}{\lambda}\right), \qquad \varepsilon = 0.025. \tag{9}$$

Numerical simulations with periodic boundary conditions applied over a box of size twenty one unit cells ($L = 21\lambda$) show that the composite surface still supports stable traveling wavetrains, see Figure 3. The reason for the choice of the particular parameter settings is historical: these simulations, along with other types of complicated dynamic behavior over composite surfaces were first reported in [3, 40].

The wavetrains will now have a superimposed small scale modulation; this is because of periodic spatial variations in the medium that they sample as they travel; with a slight abuse of terminology we will call them "wiggling pulses". A typical startup transient to such a wiggling pulse is given in Figure 3. The panels show (from left to right) the evolution of a pulse-like initial profile (leftmost panels, $u$ above and $w$ below) towards a typical snapshot of the final, left-travelling in this case, wiggling pulse. The medium heterogeneity (variation of $b(x)$) is given at the bottom of each panel to guide the eye. One can discriminate two stages in the transient. The first stage involves the development – starting from the smoooth initial condition – of localized "wiggles"; this development occurs on a relatively fast time scale. The second stage involves gradual approach to an attracting, propagating, wiggling pulse; the time scale for this gradual approach is relatively slower. The ultimate attracting solution (for a periodic medium) is characterized by two frequencies; one is related with modulation of the pulse as

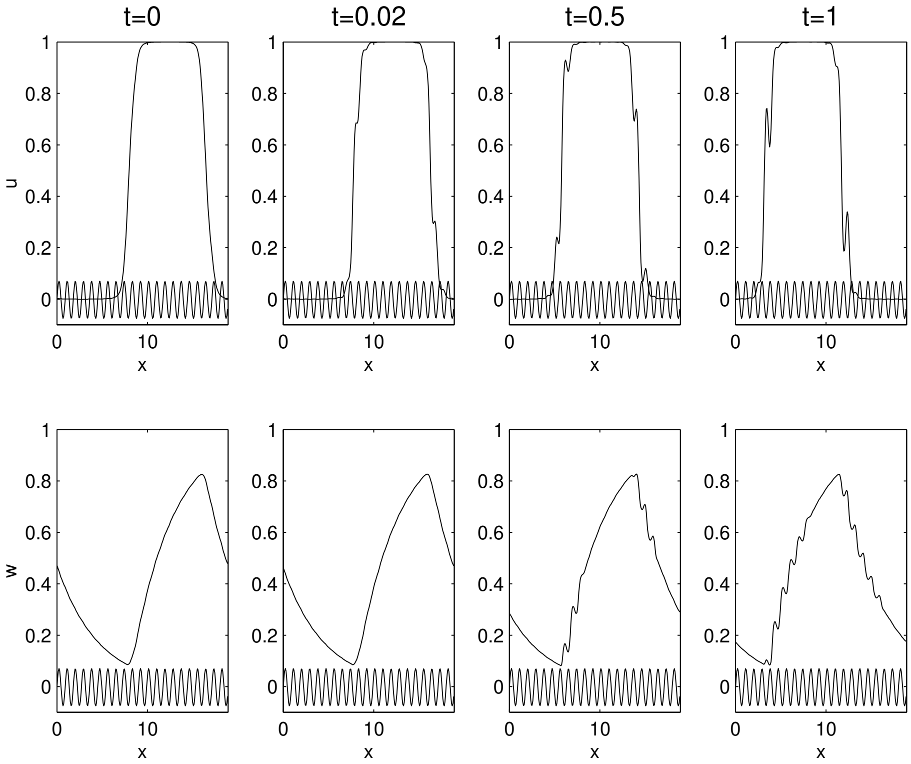


Figure 3: Typical solution of (7) with the choice of coefficients in (9). Pulse moving to the left. Variations in $b(x)$ overlayed.

it traverses one unit cell of the heterogeneity - the other is related to the size of the entire box. If we travel with the average speed of the wiggling pulse, then we see only one frequency: an oscillatory frequency (the "wigging" frequency) that is associated with the destruction and reformation of the wiggles as the pulse travels one cell to the left (as in this case) or to the right. The important thing for the moment is that, if we "ignore" or "average out" the wiggling, this can be thought of as a *coarse traveling pulse*: a pulse which, viewed coarsely, has constant speed and constant shape.

The obvious question is: can one obtain an (averaged) equation whose *exact* solution is a good approximation of the (coarse) pulse with the correct (average) speed? Homogenization [4] provides a systematic approach to deriving such an equation in the limit $\lambda \to 0$; a hierarchy of equations containing higher order corrections in $\lambda$ can also be systematically derived. More recently exponential (asymptotic beyond all orders) corrections have also been obtained for parabolic as well as hyperbolic PDEs [18, 21] – and shown to be crucial in understanding the phenomenon of wave pinning in discrete media [18, 23]. For parabolic PDEs the issue of convergence of the attractors of the approximate equations to the

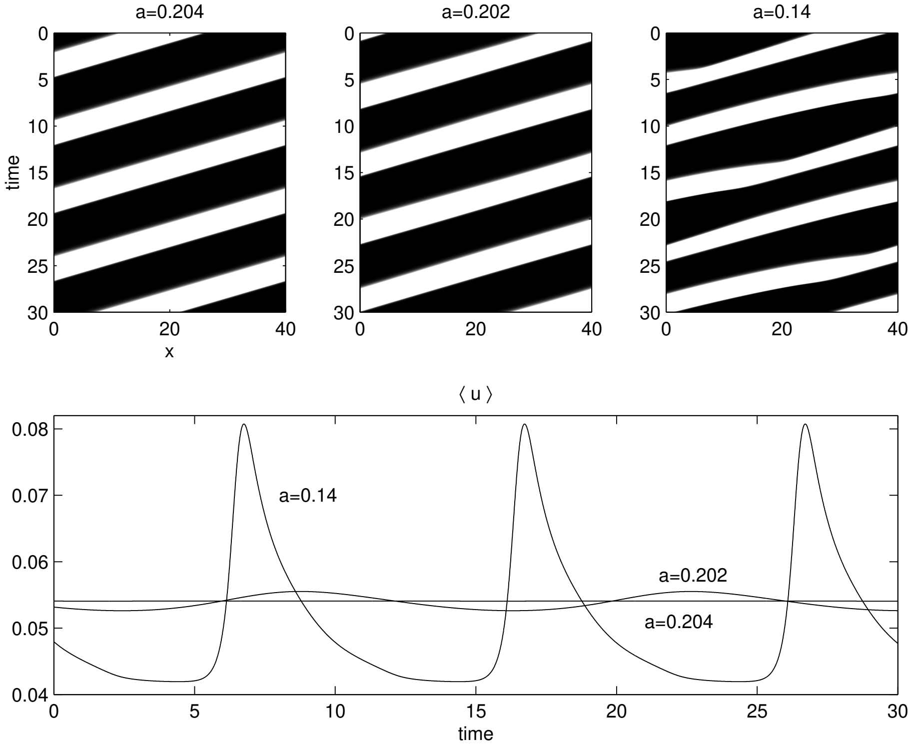


Figure 4: Bifurcation from a steady pulse to a modulated, "breathing", pulse in uniform media ($b = \text{const} = -0.025$, $L = 40$, $\varepsilon = 0.025$) as the parameter $a$ changes.

attractors of the detailed ones at the limit of $\lambda \to 0$ is the subject of intense current research, [12, 11].

Our ambition is to circumvent the explicit derivation of such approximate (effective, coarse) equations. The proposed procedure aims at computationally extracting the long-term effective dynamics without first obtaining such equations and subsequently analyzing them. We will go beyond computing a few effective attractors in our illustration; we will demonstrate that the procedure is capable of following the (coarse) dependence of effective attractors on system parameters (including $\lambda$) and of identifying *effective bifurcations*. We will do this in a context where the "effective bifurcation" in question has a well-defined counterpart in the detailed problem, so that the "effective" and the true bifurcations can be compared.

Before we describe this "coarse bifurcation", and since we have described constant shape traveling pulses in homogeneous systems, let us also describe *modulated traveling pulses* in homogeneous systems (e.g. [5]). Constant shape traveling pulses in homogeneous systems may undergo a Hopf bifurcation in the co-moving frame, resulting in a modulation of their instantaneous shape and speed, see Figure 4; if we move with the correct average speed, we see a nontraveling, modulated, "breathing", pulse that acquires the same shape after one modulation period.

It was observed in [3] that, with the choice (9), the heterogeneous system (7) undergoes a similar type of bifurcation, from a "wiggling pulse" to a "breathing wiggling pulse": a pulse which not only wiggles in a small, fast scale as it goes over each heterogeneity unit cell, but which also modulates its overall shape and speed at a much longer timescale. This is (in a comoving frame) a Neimarck-Hopf bifurcation from a periodic (wiggling) solution to a quasiperiodic (wiggling *and breathing* solution) with the concomitant frequency lockings that one expects for dynamics on invariant tori. Finding this bifurcation for the full system is an exercise in numerical Floquet theory. We have performed this exercise for the detailed system, and have found that the (detailed) primary Hopf bifurcation of a wiggling to a wiggling-breathing pulse occurs at $\lambda \approx 0.988$. We have accurately computed this Neimark-Hopf bifurcation through a shooting code applied on a spectral discretization of the governing PDE; Newton-Raphson iterations, employing a monodromy matrix computed through integration of the variational equations using ODESSA [29], converged on the fixed point of a Poincaré map transverse to the limit cycle. A pinning condition was used to compute the pulse speed, and the leading Floquet multipliers were numerically obtained from the monodromy matrix upon convergence; the numerical value of the Floquet multiplier at unity was used as a numerical accuracy check. A pair of (complex conjugate) Floquet multipliers exits the unit circle (as we vary $\lambda$ at $\lambda_0 \approx 0.988$), and a subsequent secondary Neimark-Hopf bifurcation occurs at $\lambda_1 \approx 1.024$ as a second complex conjugate pair exits the unit circle, making the wiggling pulse doubly unstable.

A small point worth noting is that we initially solved the fixed point problem over the entire 21-stripe, $21\lambda$-long domain; it is easy to see, however, that – since the pulse after traveling one stripe is a spatial shift of itself by $\lambda$ – there is an easier way of solving the problem. One can find the fixed point of a process involving integration over the time that it takes to traverse one stripe composed with a spatial shift by $\lambda$. Our original monodromy matrix $M$ is then equal to $(\mathcal{S}_\lambda J)^{21}$, where $\mathcal{S}_\lambda$ is the spatial shift operator by $\lambda$ and $J$ is the result of integrating the variational equations over the same (one-stripe-traversing) time. The top three frames of Figure 5 show space-time plots of the wiggling pulse just before the bifurcation, just after the bifurcation, and considerably after the bifurcation; the breathing is practically invisible in the second of the three subfigures and visually discernible with some difficulty in the third one. It is much easier to observe the bifurcation in the frame in the middle of Figure 5 where the spatial average,

$$\langle u \rangle(t) := \int_{\mathbb{R}} u(t,x)dx, \tag{10}$$

is plotted as a function of time. It is periodic ("coarsely steady") at $\lambda < \lambda_0 \approx 0.988$, quasiperiodic ("coarsely periodic") with a small amplitude breath-

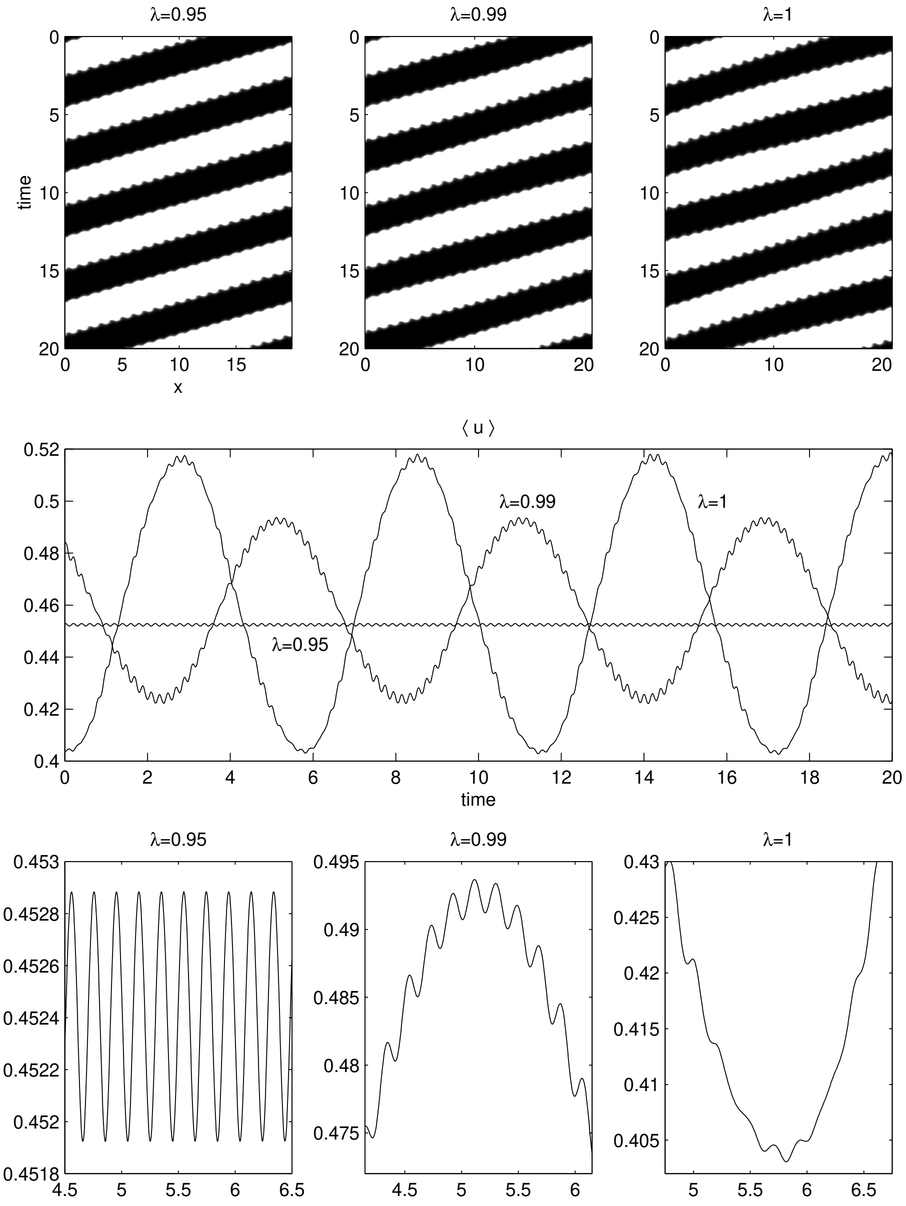


Figure 5: The "coarse Hopf bifurcation".

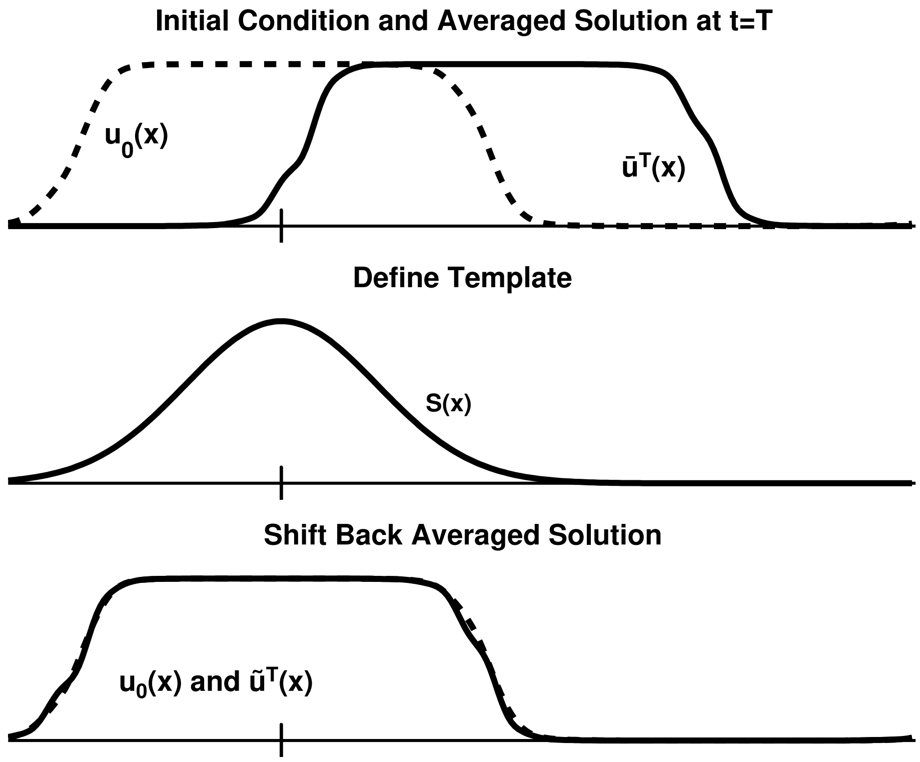


Figure 6: Pinning-shift using template fitting.

ing modulation at $\lambda = 0.99$ and still quasiperiodic ("coarsely periodic") but with a larger amplitude breathing modulation at $\lambda = 1.00$. The bottom row of Figure 5 shows blowups of these three curves stressing the different length and time scales of the wiggling and the breathing modulations. The middle frame of Figure 5 clearly suggests a "coarse" view of this transition as the classical (Poincaré-Andronov-Hopf) bifurcation of an effectively traveling to an effectively modulated pulse, as opposed to the true (Neimark-Sacker-Hopf) bifurcation of a wiggling pulse to a breathing-wiggling pulse with the concomitant (but systems level uninteresting) details of small scale variations, resonances and Arnold horns. We will perform the (effective) bifurcation analysis directly on the coarse features of the solution; we expect our procedure to capture this "coarse Hopf" bifurcation, but filter out the fine scale perturbations. While this will be done for the case of our "finely periodic" heterogeneous medium, we expect that – under reasonable assumptions – the procedure is general enough to be able to handle effective bifurcations for a large class of spatial inhomogeneities in a systematic way.

### 4.0.1 Pinning Shift

The averaged solution $\bar{u}$ is a (practically) constant shape moving pulse, but in order to use RPM we must formulate the problem as a fixed point problem. We therefore factor out the movement of $\bar{u}$ along orbits of the continuous symmetry group (the translational invariance due to the periodic boundary conditions). This is done through a procedure based on *template fitting*, see [36], which pins the traveling pulse at a fixed $x$-coordinate (a fixed phase along the group orbit). We call the pinning-shift operator $\mathcal{S}$ and after introducing a template function $S(x)$, we let $\tilde{u} = \mathcal{S}\bar{u}$ be the shifted version of $\bar{u}$ that best fits $S(x)$, in the sense that

$$\tilde{u}^T(x;\lambda) = \mathcal{S}\bar{u}^T(x;\lambda) \equiv \bar{u}^T(x+c;\lambda), \qquad c = \arg\max_{c' \in \mathbb{R}} \int_{\mathbb{R}} \bar{u}^T(x+c';\lambda)S(x)dx. \tag{11}$$

This pinning shift is schematically illustrated in Figure 6. It allows us to look (using RPM) for fixed points of the composition of the coarse time-stepper with the pinning-shift operator $\mathcal{S}$,

$$u_0(x) = \tilde{u}^T(x;\lambda)|_{u_0(x)} \equiv \mathcal{S}\bar{u}^T(x;\lambda)|_{u(0,x,s;\lambda)=u_0(x)}, \tag{12}$$

with $u(t,x,s;\lambda)$ as in (3) (for fixed $\lambda$). Upon convergence of the RPM the effective pulse speed $v$ can be deduced from the converged value of $c$ and the RPM time reporting horizon $T$ simply by taking $v = c/T$.

# 5 Numerical results

As described in Section 4 above, the computational domain for our numerical experiments is the interval $[0, L]$, where $L = 21\lambda$, with periodic boundary conditions. There are many parameters that could be used in a bifurcation study. We chose to use as a bifuration parameter the heterogeneity size $\lambda$ itself, to study the bifurcation described in Figure 5, and to illustrate that our approach is capable of promising results away from the $\lambda \to 0$ limit. With $L = 21\lambda$, we study relatively long-wavelength wavetrains, as compared to true pulses, arising in infinite domains.

Since the $x$-dependence of the right hand side in (7, 8, 9) (corresponding to $F$ in (5)) is periodic with period $\lambda$, it is clear from (3) that $u(t,x,s)$ is periodic in $s$ – the spatial shift, which also parametrizes our ensemble – with the same period. The definition of $\bar{u}^T(x;\lambda)$ in Section 2 therefore reduces to

$$\bar{u}^T(x;\lambda) = \frac{1}{\lambda}\int_0^\lambda u(T,x,s;\lambda)ds, \tag{13}$$

where $u(T,x,s;\lambda)$ is the result of integrating (7, 8, 9) with some initial condition $u_0(x)$ to time $T$, as in (3). As we mentioned above, we use RPM to solve the fixed point problem (12),

$$u_0(x) - \tilde{u}^T(x;\lambda)|_{u_0(x)} = 0, \tag{14}$$

where, as we discussed,

$$\tilde{u}^T(x;\lambda)|_{u_0(x)} \equiv \mathcal{S}\bar{u}^T(x;\lambda)|_{u(0,x,s;\lambda)=u_0(x)} \tag{15}$$

and $\mathcal{S}$ is the pinning-shift operator. The solution to (14) is what we call the coarse solution. The direct solution of (7, 8, 9) is the detailed solution.

We have slightly abused our notation here; $u$ in equations (12)–(14) is the entire vector of dependent variables. Since our sample problem is a system of two coupled equations, the $u$ in (12) has two components, the variables $u$ and $w$ of (7, 8).

## 5.1 Implementation

Before we present the coarse bifurcation results with respect to the parameter $\lambda$ in (9), we discuss a couple of relevant details for our particular implementation. We discretize $[0, L]$ using a uniform finite difference mesh with $N$ points; integrations are performed with a Crank-Nicolson method (the nonlinear terms are treated explicitly) with a constant time step $\Delta t$. The discretization is fine enough ($N = 256$, $\Delta t = 1/256$) and the convergence tolerance `tol` in RPM is small enough (`tol`$=10^{-10}$) so that we can consider the simulation results as converged/accurate with respect to the discretization. We approximate the integral (13) numerically with the trapezoidal rule,

$$\bar{u}^T(x;\lambda) \approx \frac{\Delta s}{\lambda}\sum_{n=0}^{N_s-1} u(T,x,n\Delta s;\lambda), \qquad \Delta s = \frac{\lambda}{N_s}. \tag{16}$$

We hence run up to reporting horizon $T$ with the Crank-Nicolson time-integrator $N_s$ times, shifting the material $\Delta s$ spatial units each time. Finally we average over the results, cf. Figure 2. Note that the trapezoidal rule is exponentially accurate by the periodicity of $u$ in $s$.

For the pinning-shift some care must be taken. Again, let $\mathcal{S}$ be the pinning-shift operator defined in (11), such that $\tilde{u}^T := \mathcal{S}\bar{u}^T$. Clearly, $\mathcal{S}^2 = \mathcal{S}$. It turns out to be important that also our numerical shift operator, $\tilde{\mathcal{S}}$, satisfies this property exactly. Otherwise, the numerical approximation of $\tilde{u}^T$ may not help us converge to a coarse steady state. For a naive implementation of $\tilde{\mathcal{S}}$, based on numerical integration and shift with interpolation, typically $\tilde{\mathcal{S}}^2 \neq \tilde{\mathcal{S}}$. We take the template $S(x) = \cos(2\pi x/L)$ and compute the inner product in (11),

$$\frac{1}{L}\int_0^L \bar{u}^T(x+c';\lambda)S(x)dx = \sum_k \hat{u}_k^T(\lambda)\frac{e^{ikc'}}{2\pi}\int_0^{2\pi} e^{ikx}\frac{e^{ix}+e^{-ix}}{2}dx, \tag{17}$$

where $\hat{u}_k^T(\lambda)$ are the Fourier coefficients of $\bar{u}^T(\,\cdot\,;\lambda)$. Since $\bar{u}^T$ is real, $\hat{u}_k^T(\lambda) = \overline{\hat{u}_{-k}^T(\lambda)}$, and we obtain

$$\frac{1}{L}\int_0^L \bar{u}^T(x+c';\lambda)S(x)dx = \mathrm{Real}\left(\hat{u}_1^T(\lambda)e^{ic'}\right). \tag{18}$$

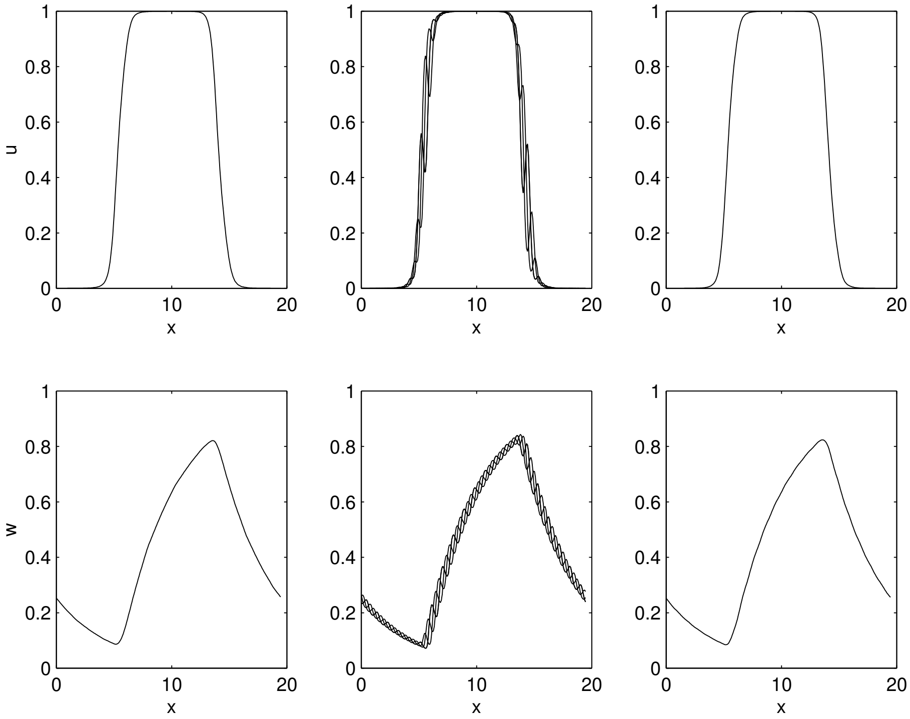


Figure 7: Comparison of coarse and detailed solution. Left frame: steady state solution of coarse time-stepper. Middle frame: snapshots of solution shape on the limit cycle of the detailed solution. Right frame: average of the solution shape on the limit cycle (snapshots in middle frame).

Hence $c$ in (11) should be chosen such that $\hat{u}_1^T(\lambda)e^{ic}$ is real. Numerically we can efficiently compute the $N$ coefficients $\hat{u}_k^T(\lambda)$ of $\bar{u}^T(\cdot;\lambda)$ via the Fast Fourier Transform, and define $\tilde{\mathcal{S}}$ as

$$\tilde{\mathcal{S}}\bar{u}^T(x;\lambda) := \sum_{k=-N/2+1}^{N/2-1} \hat{u}_k^T(\lambda)e^{ik(x+c)} \qquad \text{such that} \qquad \mathrm{Imag}\left(\hat{u}_1^T(\lambda)e^{ic}\right) = 0. \tag{19}$$

For this implementation, $\tilde{\mathcal{S}}^2 = \tilde{\mathcal{S}}$.

## 5.2 Results

The results reported in this section were obtained with $N_s = 5$ (5 shifted copies) and time horizon $T = 0.5$, unless otherwise stated. The first result is that a branch of fixed points for our procedure does indeed exist in the relevant parameter range. The shape of these fixed points does visually correspond to the coarse (locally averaged) detailed traveling solutions (see Figure 7); their speeds also correspond to the average speed of the detailed traveling solutions. What is particularly encouraging, is that so does their stability: we do observe two successive "coarse Hopf" bifurcations, where a "coarse modulation" frequency is born. We will document below that the bifurcating "coarse frequencies" correspond quite accurately to the secondary Hopf bifurcations that the detailed solution undergoes.

The first bifurcation value for our scheme is obtained at $\lambda = \lambda_0^c \approx 0.959$ while the second instability arises at $\lambda = \lambda_1^c \approx 0.996$. Figure 8 shows a comparison of the two bifurcation diagrams (detailed versus coarse) plotted in terms of $\langle u \rangle$ versus $\lambda$ (top) and mean speed of propagation $v$ versus $\lambda$ (middle). Solid curves correspond to stable solutions. For the coarse problem, these are constant travelling shapes, while for the detailed problem, what is plotted is one snapshot (on a Poincaré map) of the periodic detailed solution; the period of the detailed solution corresponds to travelling over a unit cell of the heterogeneity. With the same interpretation, dashed lines correspond to unstable solutions after the first instability (a "coarse Hopf" for the coarse problem, and a secondary Neimark-Sacker bifurcation to a torus for the detailed problem). Similarly, dotted lines correspond to doubly unstable solutions after the second instability ("coarse Hopf"concl/Neimark-Sacker again respectively). RPM-type methods can also be used to converge on fixed points of the Poincaré return map, [30, 34, 31], and we are currently working on using these methods to trace the coarse modulated branches themselves.

The bottom frame of Figure 8 shows a comparison of the largest eigenvalues of the linearization of our coarse time-stepper at its fixed point with the corresponding quantity from the detailed problem. The first snapshot shows the time-stepper eigenvalues just before the first coarse Hopf bifurcation (two pairs inside the unit circle); there also exists an eigenvalue at 1 which corresponds to the coarse translational invariance, and which does not appear because it has been removed by our pinning-shift procedure. The second snapshot is taken between $\lambda_0^c$ and $\lambda_1^c$ (one pair of time-stepper eigenvalues has crossed, while the second pair is still stable, inside the unit circle). Finally, the third snapshot is taken after the second coarse Hopf bifurcation, showing two unstable pairs, and a third one (still stable, but quickly approaching a third instability).

Figure 10 shows the eigenvector corresponding to the instability (the coarse "breathing" modulation of the traveling wave). Actually shown is the $u$ component of the real and imaginary parts of the complex eigenvector; we see that it is localized at the front and back of the coarse pulse, and that (as we expect) it has no "wiggles".

What "fine" quantity should the multipliers in Figure 8 be compared to? The detailed travelling/wiggling solution, is periodic over the entire box size of $21\lambda$. We compute numerically, through our full shooting code, the spectrum of the monodromy matrix of this limit cycle; the coresponding Floquet multipliers $\mu_i$ and Floquet exponents $\sigma_i$ are related through $\mu_i = \exp(\sigma_i T_{21})$, where $T_{21}$ is the overall period, the time it takes the wave to traverse all 21 stripes. The quantity we really want is $\exp(\sigma_i T)$, where $T$ is our RPM reporting horizon. We could extract the Floquet exponents from the full monodromy matrix, but

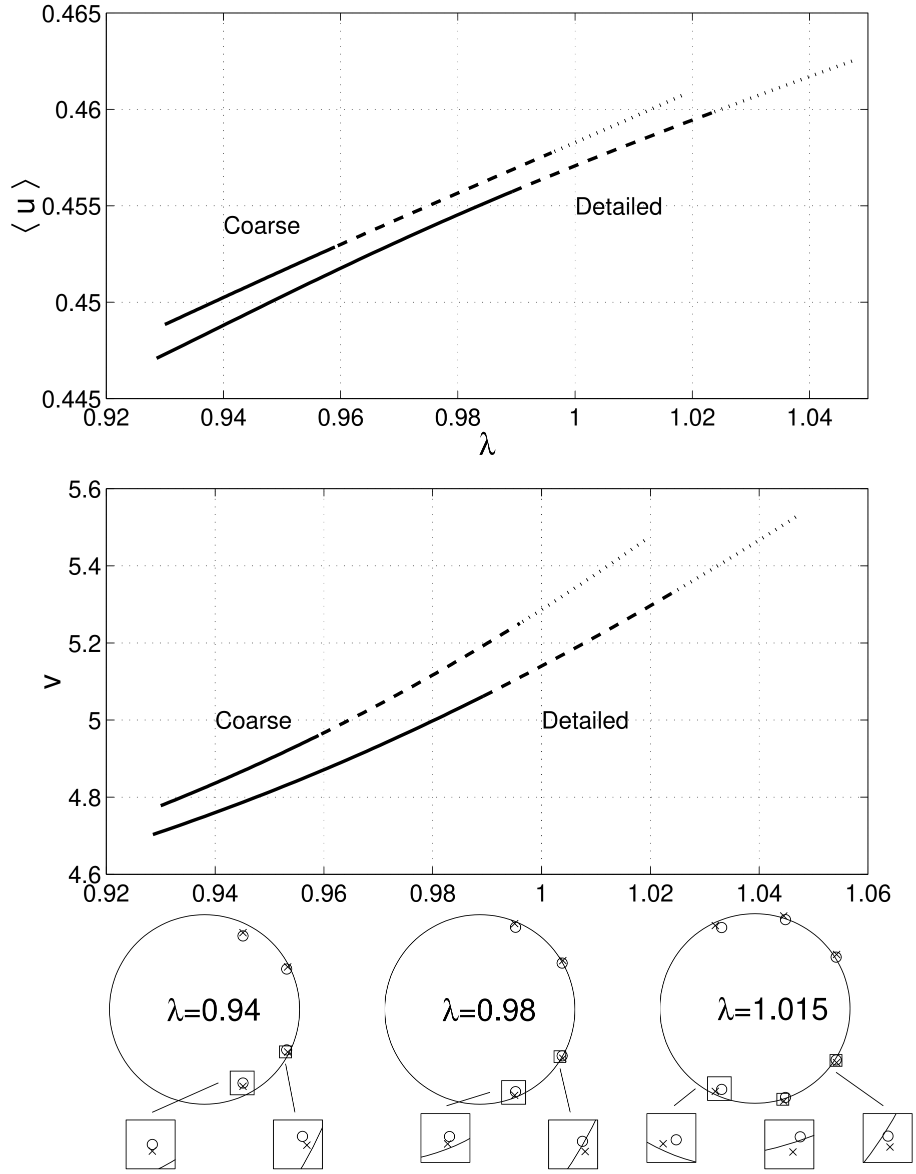


Figure 8: Bifurcation diagram for coarse and detailed equations. Top frame: spatial $u$ average, $\langle u \rangle$, as a function of $\lambda$. Middle frame: mean speed of propagation, $v$, as a function of $\lambda$. Bottom frame: largest eigenvalues for different $\lambda$: circles – limit cycle, crosses – RPM.

the large overall period can lead to inaccuracies, especially regarding the choice of the correct imaginary part. Referring back to the discussion in Section 4, we compute instead the Floquet exponents from the eigenvalues $\exp(\sigma_i T_1)$ of the matrix $\mathcal{S}_\lambda J$, the $21^{\text{st}}$ roots of the eigenvalues of the full monodromy matrix. Using these to compute $\sigma_i$, the circles in Figure 8 are centered at $\exp(\sigma_i T)$. Clearly, the first and second bifurcating coarse modulation frequencies for our procedure are very closely matched to the corresponding bifurcating frequencies in the detailed problem.

We close the results section with a discussion of the effect on the computations of the RPM reporting time-horizon $T$. As we have discussed above, as long as $T$ lies within reasonable bounds (long enough for the correct "wiggles" to develop, but also not far too long for coarse instabilities to "explode"), it should not affect the results. For our problem, the "time for the correct wiggles to develop" can be eyeballed to be of the order of 0.05 for the $u$ component (see Figure 3). In the context of hydrodynamic limits of the moments of kinetic simulations, this corresponds to the time for the higher moments to become functionals of the lower ones. The reporting time-horizons we chose were considerably longer (0.25, 0.5, 1.0). Figure 11 and Table 1 show the relatively small effect of reporting time horizon on the first coarse bifurcation value: $T = 0.25$ gives a result that is not yet converged, while $T = 0.5$ and $T = 1$ give more or less the same bifurcation point. This may be explained due to the slower development of wiggles on the $w$ profile of the solution.

The dependence of the bifurcation results as the number of copies in the ensemble and the reporting horizon grow are also quantified in Table 1. The convergence is exponential in the number of copies (which is expected, as mentioned above, by the periodicity of the spatial shift and the trapezoidal rule for averaging) – very accurate values are obtained already for small $N_s$. A couple of more issues are touched upon in Table 1. When $N_s = 1$ we started the pulse at two different locations on the striped medium: at the beginning of a stripe ($\alpha = 0$) and in the middle of a stripe ($\alpha = \lambda/2$). We notice that the bifurcation point depends significantly on where we start the pulse. This remained true when we added filtering to the time-stepper. In this case we filtered the pulse after time $t = T$, but before shifting back. The filter was based on Slepian sequences of length 20 to minimize ripple artifacts. As $N_s$ grows the dependence of the bifurcation on the details of the mesh quickly disappears, making the coarse solution practically translationally invariant.

# 6 Conclusion

We have introduced, in this paper, a computational approach to the study of effective behavior in complicated media. In particular, using as our main tool the "coarse time-stepper", we have shown how to analyze coarse long-term dynamics and compute coarse bifurcation behavior for such media. The basic premise for this procedure is that an effective equation for the coarse behavior exists and closes, even though it may be unavailable in closed form. Given

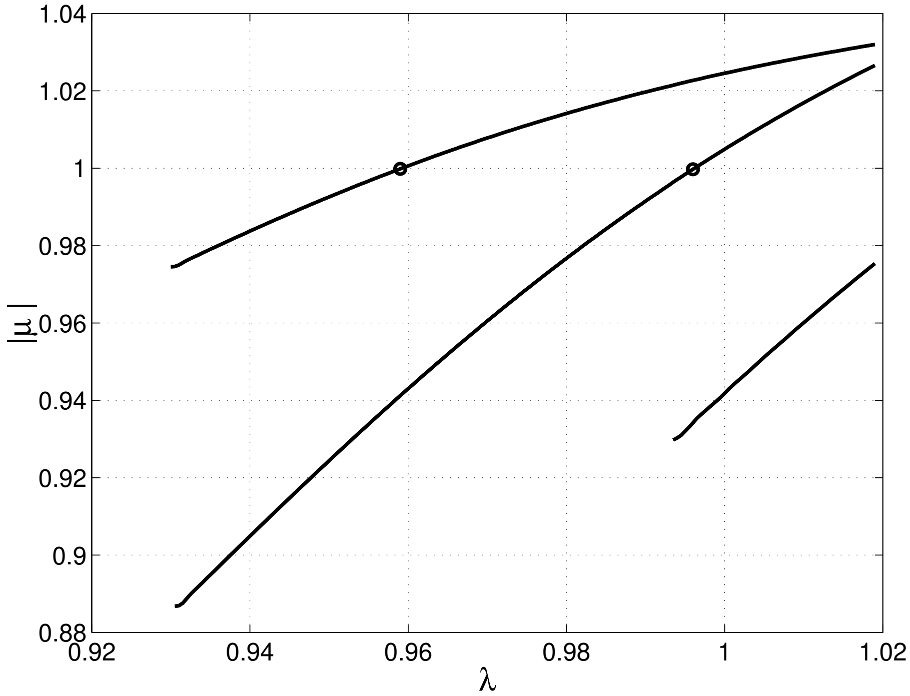


Figure 9: The absolute value of the largest eigenvalues, as computed by RPM. Note the two bifurcation points at $\lambda_0^c \approx 0.959$ and $\lambda_1^c \approx 0.996$.

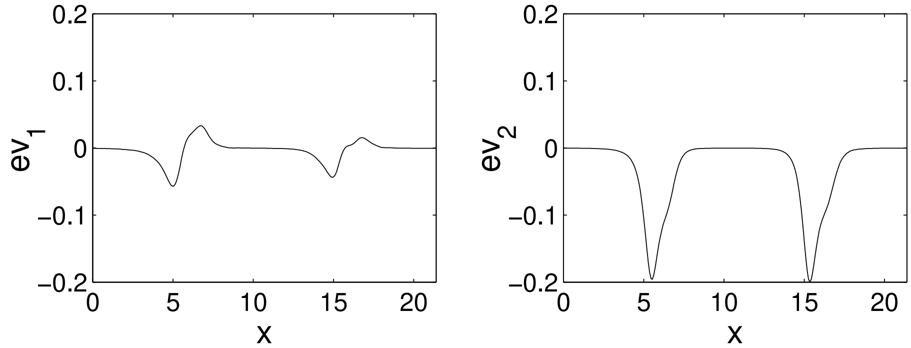


Figure 10: The $u$ part of the eigenvectors corresponding to the largest (complex conjugate) eigenvalues at $\lambda = 1.090$.

| | $T = 0.25$ | $T = 0.5$ | $T = 1.0$ |
|---|---|---|---|
| $N_s = 1$, $\alpha = 0$ | 0.94375 | 0.92505 | 0.95641 |
| $N_s = 1$, $\alpha = \lambda/2$ | no bif. | 1.02203 | 0.95762 |
| $N_s = 1$, $\alpha = 0$, filtered | 1.01802 | 0.94549 | 0.96090 |
| $N_s = 1$, $\alpha = \lambda/2$, filtered | 1.06157 | 1.00521 | 0.95260 |
| $N_s = 2$ | 0.98021 | 0.95770 | 0.95389 |
| $N_s = 3$ | 0.97997 | 0.95935 | 0.95423 |
| $N_s = 4$ | 0.97958 | 0.95921 | 0.95432 |
| $N_s = 5$ | 0.97971 | 0.95919 | 0.95429 |

Table 1: Bifurcation point for different parameters. For the case $T = 0.25$, $N_s = 1$, $\alpha = \lambda/2$ there was no bifurcation.

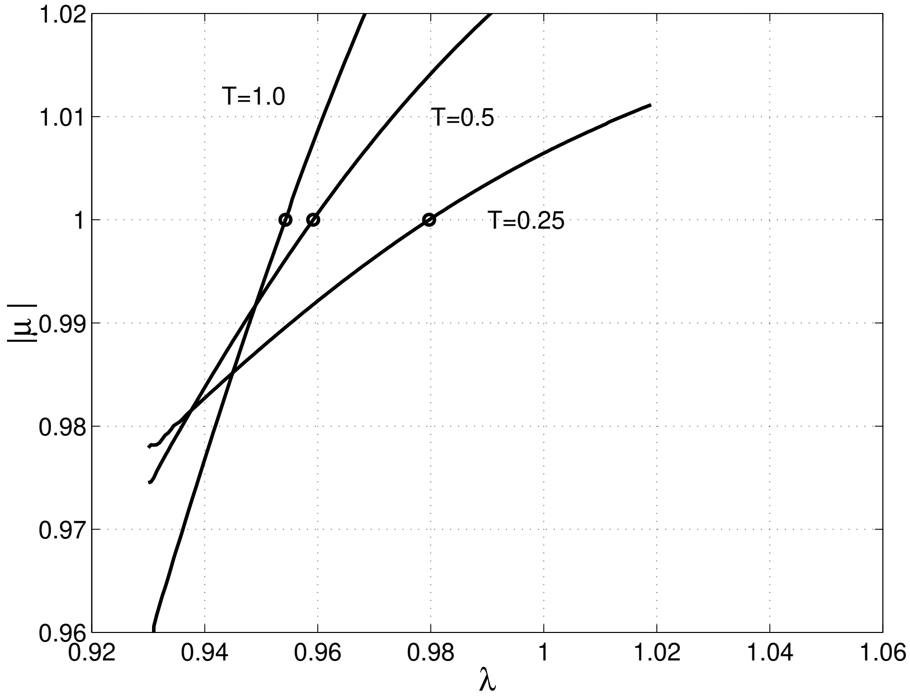


Figure 11: The absolute value of the largest eigenvalues, as computed by RPM for different $T$.

this, and given certain assumptions about separation of time scales for the (unavailable) effective equations, we exploit the so-called time-stepper based approach to bifurcation calculations (and in particular, the RPM procedure) to perform this computer assisted study. Our illustrative example consisted of a reaction-diffusion problem in a one-dimensional spatially periodic composite catalyst, and the procedure successfully captured primary and secondary coarse bifurcations that could also be computed for the detailed problem for comparison purposes. We believe that, at the appropriate limit, the time-stepper constructed through our procedure approaches the time-stepper arising from the discretization of the corresponding homogenized equations. Making this statement precise and finding the rate of the suggested approach are subjects of ongoing investigation.

Certain features of this approach are computationally attractive. The method requires, for example, the integration of several copies of the same initial condition, one for each realization of the complex medium in an ensemble of such realizations. This is trivially, and scalably, parallelizable.

The time-stepper based coarse bifurcaton analysis is conceptualy applicable to problems beyond this one; it can be used to study the coarse bifurcation structure of Monte Carlo or Lattice-Gas and Lattice-Boltzmann based simulations. It is possible that statistical mechanical ideas for, say, variance reduction in such calculations, can be used to enhance the precision of the procedure. One of the most promising features of this work is that, as long the assumptions hold, it is not restticted to the typical $\epsilon \to 0$ limit, but might also be used at higher scales. Applications of this approach to the effective bifurcation analysis of discrete problems, [20, 22], as well as to the systems level analysis of other microscopic physical models, [42, 43], is underway.

# 7 Acknowledgements

This work was partially supported by the Air Force Office of Scientific Research (Dynamics and Control) and by the National Science Foundation. I. G. K. also wishes to acknowledge the A. von Humboldt Foundation.

# References

[1] R. Balescu. *Equilibrium and Nonequilibrium Statistical Mechanics.* Wiley-Interscience [John Wiley & Sons], New York, 1975.

[2] M. Bär. *Räumliche Strukturbildung bei einer Oberflächenreaktion. Chemische Wellen und Turbulenz in der CO-Oxidation auf Platin-Einkristall-Oberflächen.* PhD thesis, Freie Universität Berlin, 1993.

[3] M. Bär, A. K. Bangia, I. G. Kevrekidis, G. Haas, H. H. Rotermund, and G. Ertl. Composite catalyst surfaces: Effect of inert and active heterogeneities on pattern formation. *J. Phys. Chem.*, 100:19106–19117, 1996.

[4] A. Bensoussan, J.-L. Lions, and G. Papanicolaou. *Asymptotic Analysis for Periodic Structures.* North-Holland, The Netherlands, 1978.

[5] H. S. Brown and I. G. Kevrekidis. Modulated traveling waves for the Kuramoto-Sivashinsky equation. In *Pattern formation: symmetry methods and applications*, volume 5 of *Fields Inst. Commun.*, pages 45–66. Amer. Math. Soc., Providence, RI, 1996.

[6] M. C. Cross and P. C. Hohenberg. Pattern formation outside of equilibrium. *Rev. Mod. Phys.*, 65(3):851–1112, 1993.

[7] E. Doedel, H. B. Keller, and J.-P. Kernévez. Numerical analysis and control of bifurcation problems. I. Bifurcation in finite dimensions. *Internat. J. Bifur. Chaos Appl. Sci. Engrg.*, 1(3):493–520, 1991.

[8] E. Doedel, H. B. Keller, and J.-P. Kernévez. Numerical analysis and control of bifurcation problems. II. Bifurcation in infinite dimensions. *Internat. J. Bifur. Chaos Appl. Sci. Engrg.*, 1(4):745–772, 1991.

[9] G. Ertl. Oscillatory kinetics and spatio-temporal self-organization in reactions at solid surfaces. *Science*, 254:1750–1755, 1991.

[10] F. Esch, S. Günther, E. Schütz, A. Schaak, I G. Kevrekidis, M. Marsi, M. Kiskinova, and R. Imbihl. Chemically resolved real-time imaging of catalytic reactions on composite surfaces. *Catal. Lett.*, 52:85–90, 1998.

[11] B. Fiedler and M. I. Vishik. Quantitative homogenization of analytic semigroups and reaction diffusion equations with diophantine spatial frequencies. Preprint A-11-2000, Freie Universität Berlin, 2000. Adv. Math., in press.

[12] B. Fiedler and M. I. Vishik. Quantitative homogenization of global attractors for reaction diffusion systems with rapidly oscillating term. Preprint A-18-2000, Freie Universität Berlin, 2000.

[13] W. J. F. Govaerts. *Numerical Methods for Bifurcations of Dynamical Equilibria.* Society for Industrial and Applied Mathematics (SIAM), Philadelphia, PA, 2000.

[14] M. D. Graham, I. G. Kevrekidis, K. Asakura, J. Lauterbach, K. Krischer, H.-H. Rotermund, and G. Ertl. Effects of boundaries on pattern formation: Catalytic oxidation of $CO$ on platinum. *Science*, 264:80–82, 1994.

[15] C. W. Horton and F. T. Rodgers. Convection currents in a porous media. *J. Appl. Phys.*, 16:367–370, 1945.

[16] L. Howle, R. P. Behringer, and J. G. Georgiadis. Visualization of convective fluid flow in a porous medium. *Nature*, 362:230–232, 1993.

[17] J. P. Keener. Homogenization and propagation in the bistable equation. *Phys. D*, 136(1-2):1–17, 2000.

[18] J. P. Keener. Propagation of waves in an excitable medium with discrete release sites. *SIAM J. Appl. Math.*, 61(1):317–334, 2000.

[19] H. B. Keller and H. von Sosen. New methods in CFD: DAE and RPM. In W. H. Hui, Y.-K. Kwok, and J. R. Chasnov, editors, *Proc. Fifth Asian CFD Conference*, pages 17–30, Hong Kong, 1995.

[20] I. G. Kevrekidis and P. G. Kevrekidis. Heterogeneous vs discrete. To appear.

[21] I. G. Kevrekidis and P. G. Kevrekidis. Pattern speed reduction in heterogeneous 1d reaction-diffusion systems. In G. A. Pnevmatikos, editor, *Proc. 13th Summer School - Hellenic Conference on Nonlinear Dynamics: Complexity and Chaos*, Order in Chaos. 2000. Submitted.

[22] P. G. Kevrekidis, I. G. Kevrekidis, and A. R. Bishop. A continuum approach to discreteness. To appear.

[23] P. G. Kevrekidis, I. G. Kevrekidis, and A. R. Bishop. Propagation failure, universal scalings and Goldstone modes. *Phys. Lett. A*, 279:361–369, 2001.

[24] Y. A. Kuznetsov. *Elements of Applied Bifurcation Theory.* Springer-Verlag, New York, second edition, 1998.

[25] E. R. Lapwood. Convection of a fluid in a porous media. *PCPS-P. Camb. Philol. S.*, 44:508–521, 1948.

[26] J. Lauterbach, G. Haas, H. H. Rotermund, and G. Ertl. Spatio-temporal pattern formation on polycrystalline platinum surfaces during catalytic CO oxidation. *Surf. Sci.*, 294:116–130, 1993.

[27] J. L. Lebowitz. Macroscopic laws, microscopic dynamics, time's arrow and Boltzmann's entropy. *Phys. A*, 194(1-4):1–27, 1993. Statistical physics (Berlin, 1992).

[28] J. L. Lebowitz, E. Presutti, and H. Spohn. Microscopic models of hydrodynamic behavior. *J. Statist. Phys.*, 51(5-6):841–862, 1988. New directions in statistical mechanics (Santa Barbara, CA, 1987).

[29] J. R. Leis and M. A. Kramer. Algorithm 658: ODESSA: An ordinary differential equation solver with explicit simultaneous sensitivity analysis. *ACM T. Math. Software*, 14(1):61–67, 1988.

[30] K. Lust. *Numerical Bifurcation Analysis of Periodic Solutions of Partial Differential Equations.* PhD thesis, Katholieke Universiteit Leuven, 1997.

[31] K. Lust, D. Roose, A. Spence, and A. R. Champneys. An adaptive Newton-Picard algorithm with subspace iteration for computing periodic solutions. *SIAM J. Sci. Comput.*, 19(4):1188–1209, 1998.

[32] S. Nettesheim, A. von Oertzen, H. H. Rotermund, and G. Ertl. Reaction diffusion patterns in the catalytic co-oxidation on Pt(110) — Front propagation and spiral waves. *J. Chem. Phys.*, 98:9977–9985, 1993.

[33] I. Prigogine, R. Balescu, F. Henin, and P. Résibois. On the dynamical derivation of equilibrium statistical mechanics. *Physica*, 26(supplement):S 36–S 48, 1960.

[34] D. Roose, K. Lust, A. R. Champneys, and A. Spence. A Newton-Picard shooting method for computing periodic solutions of large-scale dynamical systems. *Chaos Soliton. Fract.*, 5(10):1913–1925, 1995.

[35] H. H. Rotermund, W. Engel, M. Kordesch, and G. Ertl. Imaging of spatio-temporal pattern evolution during carbon monoxide oxidation on platinum. *Nature*, 343:355–357, 1990.

[36] C. W. Rowley and J. E. Marsden. Reconstruction equations and the Karhunen-Loève expansion. *Physica D*, 142:1–19, 2000.

[37] E. Schütz, N. Hartmann, I. G. Kevrekidis, and R. Imbihl. Microchemical engineering of catalytic reactions. *Catal. Lett.*, 54:181–186, 1998.

[38] M. D. Shattuck, R. P. Behringer, G. A. Johnson, and J. G. Georgiadis. Convection and flow in porous media. part 1. visualization by magnetic resonance imaging. *J. Fluid. Mech.*, 332:215–245, 1997.

[39] G. M. Shroff and H. B. Keller. Stabilization of unstable procedures: the recursive projection method. *SIAM J. Numer. Anal.*, 30(4):1099–1120, 1993.

[40] S. Shvartsman, A. K. Bangia, M. Bär, and I. G. Kevrekidis. On spatio-temporal patterns in composite reactive media. In *Mathematics of Multiscale Materials*, volume 99 of *IMA Vol. Math. Appl.*, pages 231–254. Springer, New York, 1998.

[41] S. Shvartsman, E. Schütz, R. Imbihl, and I. G. Kevrekidis. Dynamics on microcomposite catalytic surfaces: the effect of active boundaries. *Phys. Rev. Lett.*, 83(14):2857–2860, 1999.

[42] C. Theodoropoulos, Y.-H. Qian, and I. G. Kevrekidis. "Coarse" stability and bifurcation analysis using time-steppers: A reaction-diffusion example. *P. Natl. Acad. Sci. USA*, 97(18):9840–9843, 2000.

[43] C. Theodoropoulos, K. Sankaranarayanan, S. Sundaresan, and I. G. Kevrekidis. Coarse bifurcation studies of bubble flow microscopic simulations. In *Proc. third Panhellenic Chemical Engineering Conference*, Athens, Greece, May 2001. Also, manuscript in preparation.

[44] L. S. Tuckerman and D. Barkley. Bifurcation analysis for timesteppers. In *Numerical Methods for Bifurcation Problems and Large-Scale Dynamical Systems*, volume 119 of *IMA Vol. Math. Appl.*, pages 453–466. Springer, New York, 2000.